# High Resolution Ka-Band Images of a Small Tree: Measurements and Models

Hyunjun Kim, Joel T. Johnson, *Member, IEEE*, and Brian A. Baertlein

***Abstract*—Ka-band (27 GHz to 36 GHz) radar images of a 2.5-m red maple tree, measured in the Ohio State University ElectroScience Laboratory (ESL), Columbus, compact range, are presented. Radar images of the tree with and without leaves were obtained, as well as images of a 6 in diameter metal sphere obscured by the tree for investigation of attenuation effects. The large bandwidth (9 GHz) of these measurements provides a cm scale range resolution, so that backscatter from individual components of the tree canopy can be separated. In addition, measurements made as a function of azimuth angle in 0.1 degree steps allow inverse synthetic aperture radar (ISAR) images to be obtained with cm scale resolutions in down and cross range. A single scattering model, in which tree branches are represented as a deterministic collection of cylinders and leaves as a distributed collection of curved dielectric sheets, is combined with a detailed measurement of the tree geometry to provide theoretical ISAR images for comparison with the measured data. Although incomplete knowledge of tree geometry limits a direct quantitative comparison of the measured and modeled returns, a qualitative comparison of images shows that single scattering models may be sufficient for obtaining many features of foliage objects in Ka-band radar images.**

***Index Terms*—High resolution imaging, radar measurements, synthetic aperture radar (SAR).**

## I. Introduction

THE continuing development and deployment of Ka-band radar and communication systems motivates the study of foliage scattering effects at these frequencies. Although several investigations have been performed previously [1]–[4], the large bandwidths available at Ka-band were not exploited in these studies to explore range-resolved backscattering from foliage targets. While low resolution measurements or images made with smaller bandwidths [5], [6] do provide useful information on average properties of foliage scattering, they do not allow insight into the detailed scattering mechanisms responsible for foliage returns. In addition, information on average properties of foliage scattering is not sufficient for the prediction of high resolution images of foliage objects, as may be desired in radar scene simulation studies and clutter reduction algorithm development.

Theoretical models can provide some insight into scattering effects in foliage. However, efforts in the remote sensing community have emphasized lower microwave frequencies such as L- or C-band [7]–[12], where the lower available bandwidths again provide only low resolution properties of foliage backscattering. Theoretical efforts at higher frequencies have been more limited and have concentrated on scattering models for individual foliage components [7], [9], [13], [14]. The verified component models were then used in a statistical random medium model [15]–[17], again to produce predictions only of the average properties of foliage backscattering.

Several factors complicate the scattering process in foliage at Ka-band, primarily due to the small electromagnetic wavelength (8.6 mm at 35 GHz), which produces sensitivity to the small scale features of foliage objects. Thus, foliage features such as leaf curvature and branch surface roughness, which can often be neglected at lower frequencies, can provide observable scattering contributions at Ka-band. Small scale foliage structures such as small branches or needles must also be considered, since these structures may become resonant inside this frequency range. The complexity of a foliage target at these length scales clearly makes a statistical description of the medium highly desirable for modeling purposes, but a statistical description that retains the geometrical properties of a realistic foliage target is currently not available. Even with a realistic statistical description, obtaining scattering properties of scattered fields beyond coherent and incoherent averages would likely be very difficult.

A modeling approach that can avoid these problems and enable simulation of high resolution images involves a Monte Carlo procedure. An electromagnetic scattering model is applied to realizations of a foliage target type to obtain a sample of scattered fields or radar images, from which statistical properties can be deduced. Recent developments in realistic foliage simulation methods, such as the CREATION [18] or Lindenmayer system (L-system) [19] techniques, make the Monte Carlo approach possible, since realistic realizations of foliage objects can be generated. Numerically exact or approximate electromagnetic scattering models can potentially be applied, but again, the small wavelengths at Ka-band make numerically exact approaches extremely time consuming for all but the smallest foliage structures. An approximate model that has been applied in Monte Carlo simulations at lower frequencies involves a single scattering theory, with foliage branch structures represented as cylinders [20], [21]. Single scattering contributions for each cylinder are then added with an appropriate phase shift for each cylinder [22], to produce the total scattered field. In addition, [20] considered some low resolution, lower frequency images of a simulated tree.

In this paper, high resolution Ka-band images of a small tree measured in the Ohio State University ElectroScience Labora-

Manuscript received May 11, 1999; revised September 9, 1999. This work was supported by a grant from the Lockheed Sanders Corporation as part of the Army Research Laboratory's Advanced Sensor Consortium.

The authors are with the Department of Electrical Engineering, ElectroScience Laboratory, The Ohio State University, Columbus, OH 43212 USA (e-mail: hjk@esl.eng.ohio-state.edu).

Publisher Item Identifier S 0196-2892(00)02851-5.

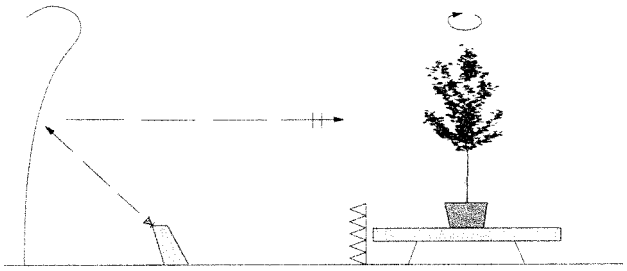

Fig. 1. Maple tree measurement configuration in the compact range.

tory, Columbus, compact range are presented. Detailed measurements of tree geometry are combined with measured image data to allow interpretation of scattering mechanisms inside the tree structure. Images were taken of the tree with and without leaves and also with a 6 in diameter metallic sphere obscured behind the tree to investigate attenuation effects. Measured images are compared with those obtained from a single scattering model similar to that of [20]. Results show that that small scale foliage features are indeed significant at Ka-band and that branch junctions can be important scatterers as well. Attenuation of an obscured target is shown to vary depending on the path through the foliage medium. Finally, the single scattering model is shown to qualitatively reproduce many of the features of measured images, so that a Monte Carlo study with a single scattering model can be useful for predicting statistical properties of high resolution foliage object images.

Measurement procedures for the study are discussed in the next section, and the model and geometrical measurements of the tree are described in Section III. Measured and modeled results are presented in Section IV and final conclusions in Section V.

## II. Measurement Procedure

The ESL compact range [23] utilizes a 4.9 m × 4.9 m Scientific Atlanta rolled edge reflector, illuminated by a TEM rectangular horn antenna at the reflector focus to obtain near-plane wave illumination of the target under test. Targets are positioned in the "quiet" zone region on a rotatable low RCS target support pedestal, and co-polarized backscattering is received by the transmitting antenna. An additional receive horn is located adjacent to the transmit horn (aligned slightly off the reflector focus) and oriented to receive the orthogonal polarization so that cross-polarized returns are also obtained. For the results presented in this paper, only vertical-polarized incidence is considered, so that only VV and HV cross sections are obtained. At Ka-band, the system can measure returns from 27 to 36 GHz in a user-defined frequency sweep. Measured returns are calibrated through 6 in diameter metallic sphere and 45° rotated dihedral target measurements for copolarizations and cross-polarizations, respectively. The effect of antenna cross polarization coupling was not removed through this procedure (copolarizations and cross-polarizations were calibrated independently), but several calibration tests showed that backscatter returns from the tree should be accurate to within approximately 1 dB.

A 2.5-m potted red maple tree was selected as the foliage target to insure a fit inside the measurement facility. The measurement configuration is illustrated in Fig. 1, and basic geometrical parameters of the maple tree are described briefly in Table I and in more detail in the next section. Fig. 2 is a photograph of the leafy tree at the time of the measurements. Measurements were performed for the tree with and without leaves to study the backscattering contributions of leaves as well as possible shadowing effects and interactions between elements. To study backscatter from a concealed target, measurements were

TABLE I
Geometrical Parameters of a Red Maple Tree

| | |
|---|---|
| Overall dimension (cm) | 250 (height) × 80 (depth) × 80 (width) |
| Main trunk height (cm) | 100 |
| Trunk diameter (cm) | 1.6 to 3.3 |
| Number of branches | 10 |
| Branch length (cm) | 50 to 80 |
| Number of sub-branches | 35 |
| Sub-branch length (cm) | 10 to 20 |
| Branch diameter (cm) | 0.2 to 1.3 |
| Number of leaves | approximately 950 |
| Leaf radius (cm) | 1 to 5 |
| Leaf thickness (cm) | 0.03 to 0.04 |
| Leaf orientation (degree) | 0 to 60 |
| Moisture content of branch | 0.5 |
| Moisture content of leaf | 0.7 |

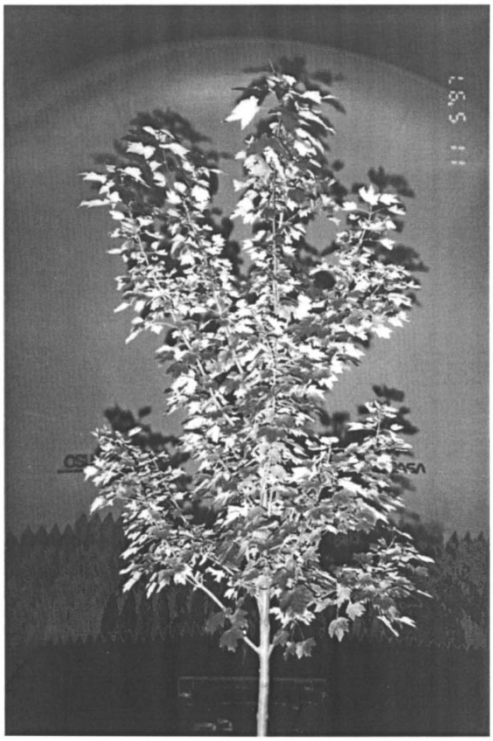

Fig. 2. Photograph of red maple tree used in measurements.

also made with the 6 in sphere calibration target, 1.2 m behind the leafy tree. For all configurations, the tree stood vertically, and absorbing fences were used to block unwanted returns from the platform and pot. Cross-polarized measurements were taken only for the bare tree case.

Backscattering measurements were taken over frequencies from 27 to 36 GHz with 10 MHz frequency steps, resulting in 900 data samples at each incident angle. A large wooden rotational platform was used to vary the incident azimuth angle from 270° to 330° and in 0.1° angle steps. These step sizes in frequency and angle were selected so that image formation with large down-range and cross-range unambiguous regions were possible. Two-dimensional (2-D) inverse synthetic aperture radar (2-D ISAR) images were formed using tomographic processing (a back projection of range profiles at several azimuth angles) following [24] with down-range and cross-range resolutions of 1.7 cm and 2.5 cm, respectively. These images correspond to a view of the tree canopy mentioned previously and will be compared to geometrical measurements of the tree in the following sections.

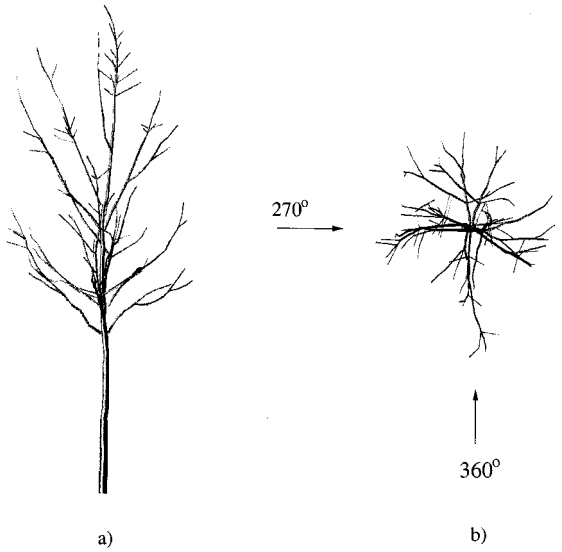


Fig. 3. Reconstructed bare maple tree with 299 cylinders: (a) Side view (b) Top view.

## III. Modeling Approach

As stated previously, the model to be applied in simulating radar images of the tree is essentially the same as that of [20]. Foliage components are represented in terms of finite dielectric circular cylinders (trunk and branches) or curved dielectric slabs (leaves), and single scattering contributions from each element are added with appropriate phase and polarization shifts depending on their location and orientation. Note that unlike [20], the influence of the ground is not considered in the model, due to the near horizontal incidence angle, and since absorbing fences were placed in front of the tree, eliminating any ground reflections or interactions.

Single scattering from finite dielectric cylinders is determined either through a physical optics [25] or eigenfunction-based [9] approach, depending on the radius of the cylinder relative to the wavelength. Doubly curved dielectric slab returns are determined through a physical optics, stationary phase method [14], [26], [27]. The advantage of using a canonical object representation is that closed-form expressions exist for scattering from these objects, greatly reducing the computational complexity. Several measurements of backscattering from foliage components at Ka-band have confirmed that these approximations are reasonable for objects with smooth surfaces [14], [28]. However, scattering from pine type branches with appreciable surface roughness were found to differ from smooth dielectric cylinder predictions. A heuristic tilted cylinder model was proposed to improve agreement for rough branches [28], but the red maple branches considered in this study did not have significant surface roughness so the smooth cylinder model was sufficient.

The main tree constituents of the red maple tree measured are the trunk, main and sub-branches, and various sizes of leaves, as described in Table I. The trunk is vertically oriented, again with no significant roughness on the bark layer except for some small protrusions on the surface. Main branches grow from the trunk and have sub-branches, to which leaves are attached. Most of the estimated 950 leaves are oriented roughly horizontally and

Fig. 4. Reconstructed leafy maple tree with 299 cylinders and 952 leaves.

have surface curvature as well as surface roughness on the order of a few millimeters. Modeling backscatter returns from a particular tree at Ka-band requires precise geometrical information for all of these foliage components. Clearly, the acquisition of every geometrical detail for all of these components would be exceedingly difficult, particularly for the smallest branches and leaves of the tree. Instead, an approximate approach was pursued, in which accurate geometrical measurements of the large scale features were made but augmented through an approximate description of leaf features.

Large scale geometrical measurements were made by creating a square grid on the floor on which the tree was placed and then dropping strings from each of 300 points on the tree to

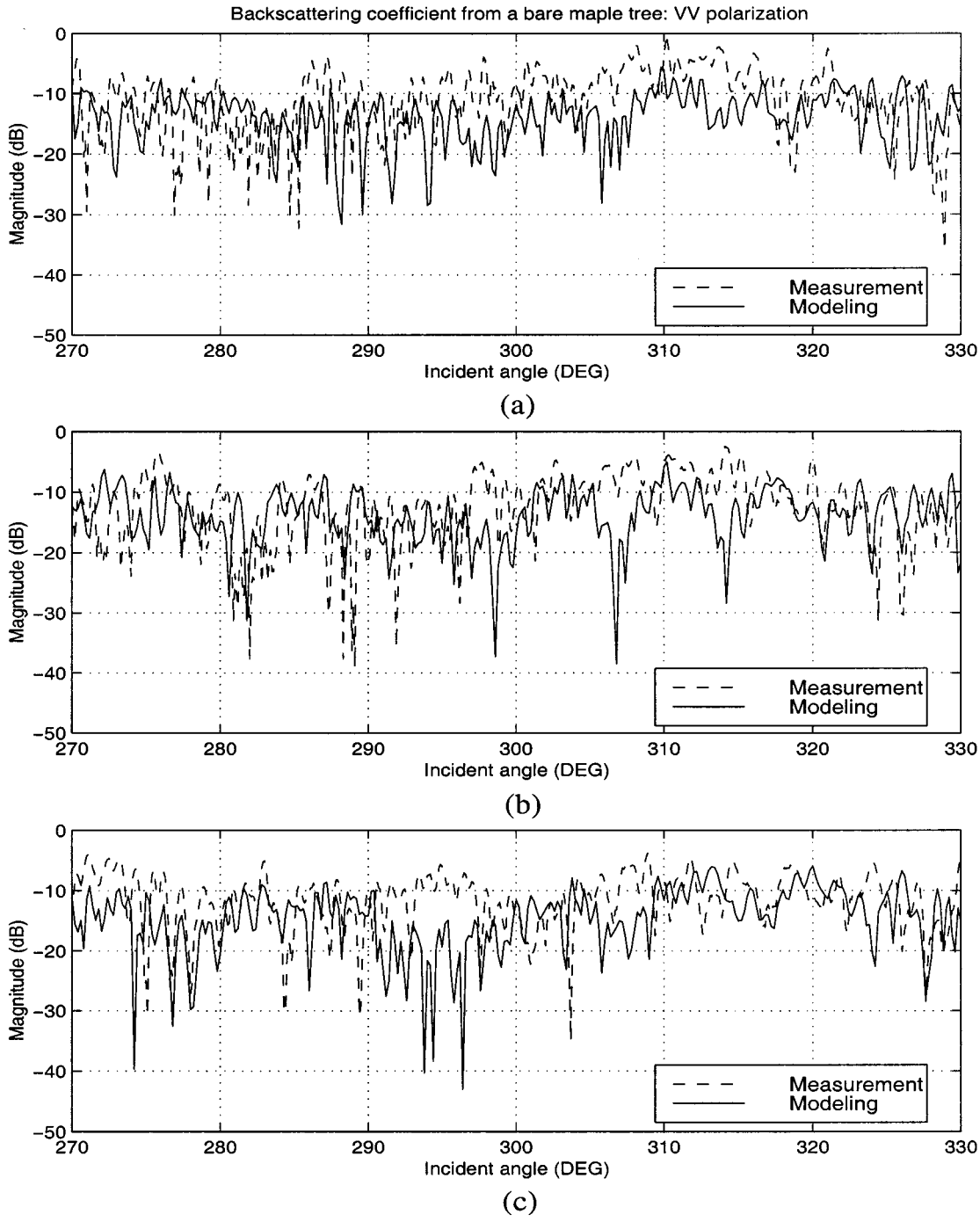


Fig. 5. Backscattering coefficient versus incidence angle for bare maple tree: (a) 35 GHz, (b) 31 GHz, and (c) 27 GHz.

allow horizontal positions to be read from the grid and height from the length of string. Radii of each branch segment were measured with digital calipers, and determined by the averaged value from two successive points. Pairs of measured points then described cylinders that make up the large scale tree structure, and were recorded along with the corresponding cylinder radii. Measurements were estimated to have less than 1 cm position error. The resulting large scale tree geometry consisted of 15 cylinders for the trunk and 284 cylinders for the branches and is illustrated in Fig. 3. Although the reconstructed tree appears very similar to photographs of the measured tree, the measurement procedure was not able to resolve the smallest branches, which are neglected in the model. Note the top view of the tree in Fig. 3 is of particular interest, because the 2-D ISAR imaging process should approximate this geometry.

The location and orientation of leaves on the modeled tree was generated through a statistical approach. Observations of typical properties of leaves on the measured tree showed their relative positions to be determined by an offset from the corresponding branches and typical elevation and tilt angles to be within 60°. Based on these observations, leaves were modeled as offset from branches by a uniformly distributed

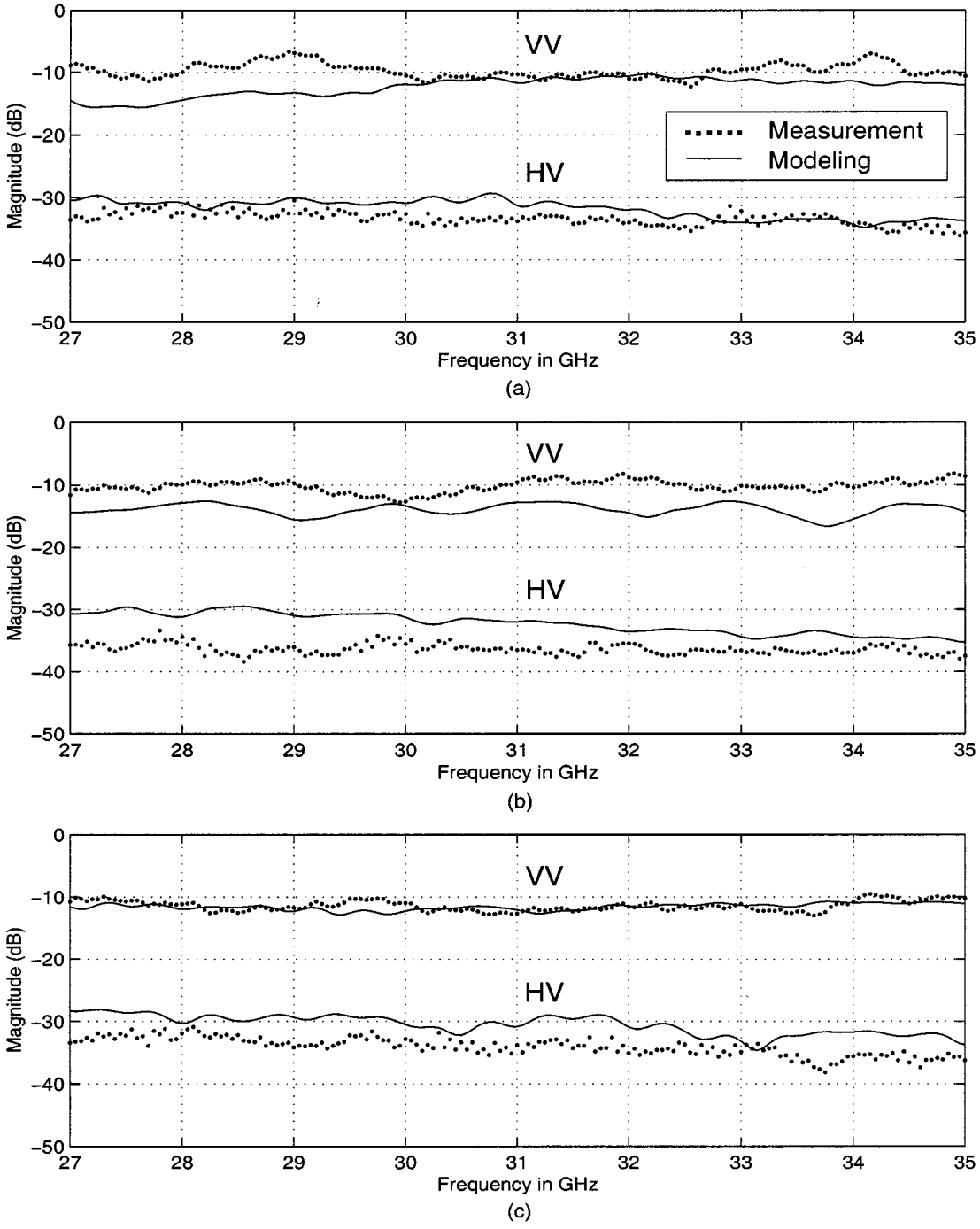


Fig. 6. Angular averaged backscattering coefficient versus frequency for bare maple tree: (a) 270°–280°, (b) 295°–305°, and (c) 320°–330°.

distance from 0 to 7 cm in both directions, while the leaf tilt angle distribution was approximated as uniform from 0° (horizontal) to 60° in elevation and uniform from −60° to 60° in azimuth. The accuracy of a uniform distribution for these parameters was not assessed, as detailed information was not available but should be reasonable for qualitative comparisons. The total number of leaves in the model was chosen to be approximately equal to the estimated number of leaves on the actual tree. Leaves were considered to be circular spherically curved disks, with a 6 cm radius of curvature and a radius modeled as 2 cm plus a uniformly distributed length that varied linearly with the corresponding branch radius. The resulting leafy tree model included 952 curved discs with radii between 2 and 5 cm and is illustrated in Fig. 4. Note that the rendering of leaves in the figure does not reproduce the curved shapes used in the scattering model.

Dielectric constants of foliage constituents were obtained from the empirical model of [29] using the water contents specified in Table I. Permittivity measurements for the red maple tree were not performed, but variations in element permittivity are not expected to contribute significantly to qualitative image features obtained by the model.

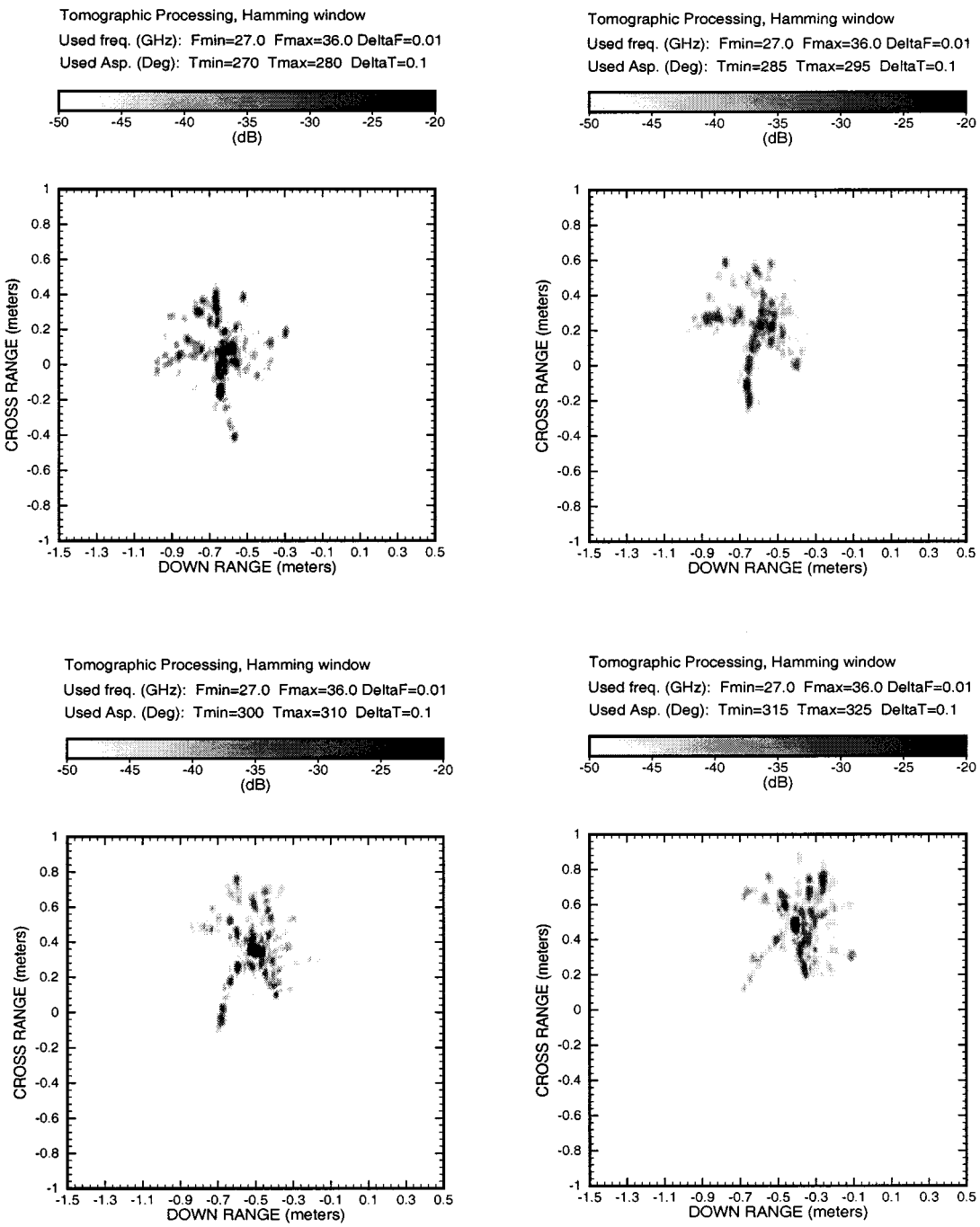


Fig. 7. Measured two-dimensional (2-D) VV ISAR images of a bare maple tree at various look angles: $\mathrm{BW} = 9$ GHz, $\delta f = 10$ MHz, $\Delta\theta = 10^{\circ}$, and $\delta\theta = 0.1^{\circ}$.

Clearly, the model developed is based on several approximations, both electromagnetic and geometrical. Electromagnetic approximations include use of physical optics techniques, neglect of diffraction, multiple scattering and shadowing effects, and possible errors in the dielectric constants assumed. Geometrical approximations include a neglect of small branches, incomplete description of leaf properties, neglect of surface roughness on the trunk and branch cm scale positioning errors. For these reasons, obtaining a detailed quantitative assessment of the single scattering model for this problem is very difficult. Both electromagnetic and geometrical sources can contribute to observed errors. Thus, a quantitative comparison of modeled and measured data will not be pursued. However, a comparison of images obtained from the model and measurements will still allow a qualitative evaluation of the single scattering theory and help to illustrate the properties of foliage scattering that a single scattering model can be expected to reproduce.

## IV. Backscatter Results and 2-D ISAR Images

### *A. Bare Maple Tree: Angular and Frequency Response of Backscatter*

Fig. 5 plots measured VV backscatter cross sections for the bare maple tree as a function of azimuth angle at three fixed

frequencies. Measured cross sections are observed to vary between $-30$ and 0 dBsm, with a $-14$ to $-15$ dBsm average over angle, which depends on the frequency. The rapid changes with azimuth angle are characteristic of constructive and destructive interference among a large number of scatterers. Higher backscattering levels are associated with azimuth angles at which larger branches are oriented broadside to the incidence direction. These measurements confirm that an average level for tree backscattering is an incomplete description when such large variations are observed.

Although again, a direct quantitative comparison of measurement and model is not warranted, it is still of interest to investigate the relationship between the two results, so model predictions are also included in Fig. 5. As expected, significant mismatches are obtained in the comparison, but it is interesting to observe that the single scattering model retains many of the characteristics of the measured results.

Fig. 6 plots angular averaged frequency responses around three aspect angles: 275°, 300°, and 325°, as defined in Fig. 3. Each plot was obtained by taking averages of both copol and cross-pol backscatter cross sections over 10° at each frequency. Copol measured cross sections in general are observed to exceed modeled results, although one of the aspect angles (320° to 330°) shows very consistent agreement between measurement and modeling. Note also that the angularly averaged backscatter shows little frequency dependence at each aspect angle. Averages taken over the entire range of angles (60°) demonstrate that measurement results are an average of 3 dB higher for copol. As discussed previously, there are several possible explanations for the observed discrepancies, including both scattering and geometrical effects. Most of these effects would tend to increase copol model predictions, so the bias appears consistent.

Cross-pol measured results in Fig. 6 are overpredicted by the model. This is somewhat surprising for a single scattering model, but radar images shown later in this section provide a reasonable explanation. It is found in the images that some of the modeled branches are in a rotated broadside orientation, resulting in large cross-pol contributions for the flat cylindrical structures considered. These large "specular"-like responses are not reproduced in the measured data, for which the branch structures are not flat cylinders. These broadside responses dominate the model predictions, resulting in a higher angular average in general. Averages of cross-pol backscatter over the entire range of angles reduces the errors within 3dB between measurements and modeling.

The next sections provide a more qualitative comparison of radar images.

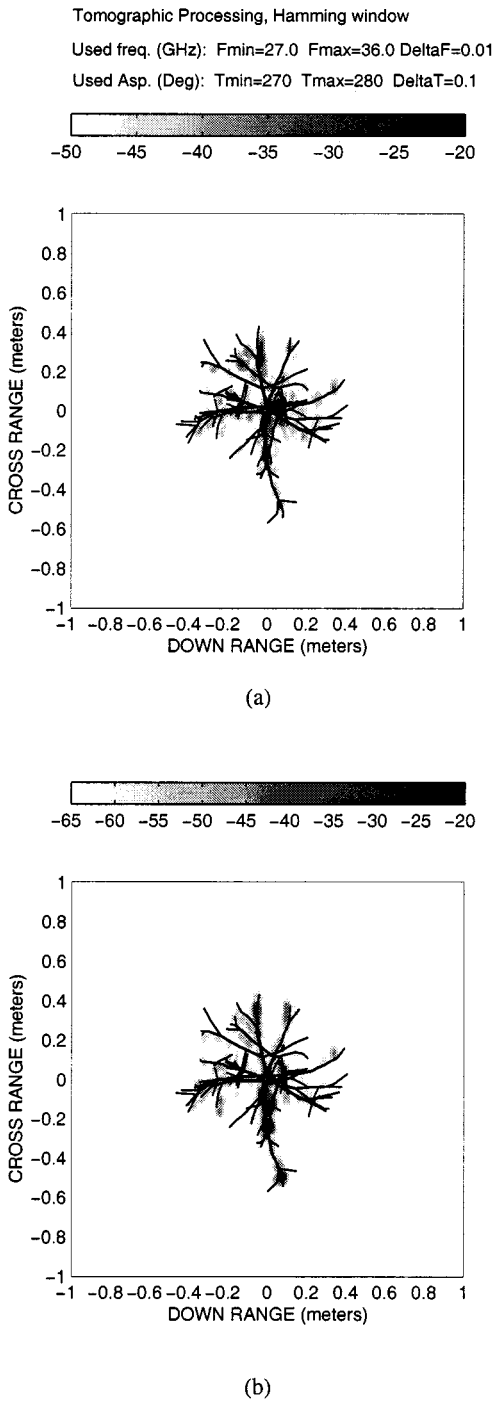


Fig. 8. Overlay of tree-top view and 2-D VV ISAR images of a bare maple tree at 270 ° look angle: $\mathrm{BW} = 9$ GHz, $\delta f = 10$ MHz, $\Delta\theta = 10°$, and $\delta\theta = 0.1°$. (a) Measured image and (b) modeled image.

### *B. Bare Maple Tree: Co-polarized ISAR Images*

Fig. 7 plots measured VV 2-D ISAR images for the bare tree at four azimuth angles. The images were formed using a 10° span of azimuth data and again with a 9 GHz bandwidth, so that resolutions of 1.7 cm and 2.5 cm were obtained in down and cross-range respectively. Use of a 10 MHz frequency step and 0.1° azimuth angle step allows sufficient unambiguous regions to avoid aliasing effects, and the anechoic chamber of the compact range eliminated large returns from all sources but the tree target. Pixel intensity is determined by the image magnitude in decibels and clearly, the resolution of the images is sufficient to identify individual foliage features. Images should be compared with the top view of the tree in Fig. 3(b), which also defines the azimuth angles referenced in Fig. 7. The relationship between Fig. 3(b) and the upper left plot in Fig. 7, which has the same azimuthal orientation, is quite striking, and illustrate that the major returns are originating from branch structures oriented broadside to the incident field as well from the central trunk. An

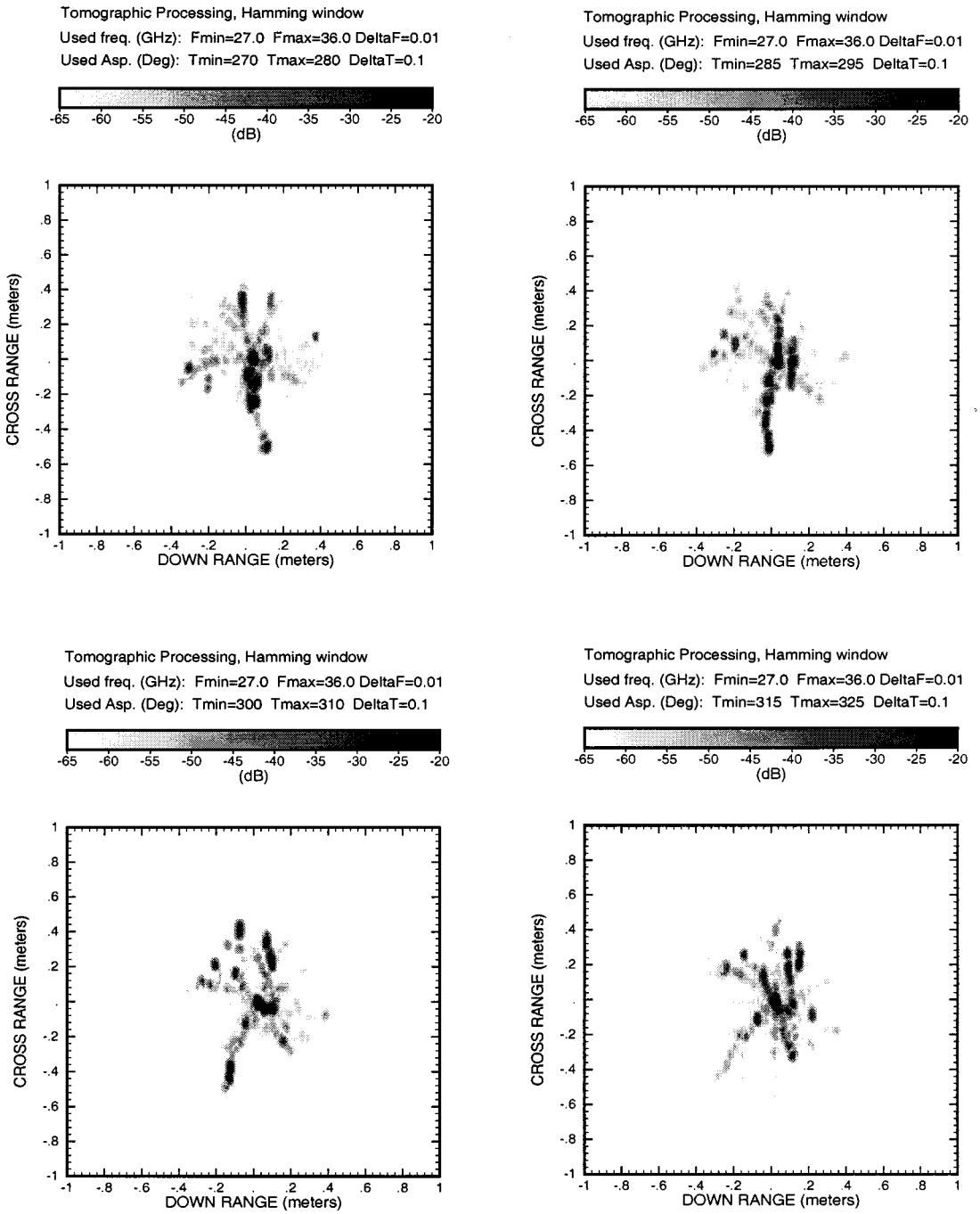


Fig. 9. Modeled 2-D VV ISAR images of a bare maple tree at various look angles: $\mathrm{BW} = 9$ GHz, $\delta f = 10$ MHz, $\Delta\theta = 10^{\circ}$, and $\delta\theta = 0.1^{\circ}$.

overlay of the image and tree structure is made in Fig. 8 and further shows that significant returns can be obtained from branch junctions (i.e., points where branches divide). Features obtained from branches on the down-range side of the tree also show that attenuation is not significant for this bare and relatively sparse tree. Images at other azimuth angles in Fig. 7 illustrate the changing contributions of individual branches as the structure rotates, again demonstrating the importance of broadside alignment. Note that the tree structure was not aligned with the axis of rotation of the platform, so the overall structure moves as the platform rotates.

ISAR images obtained from the model are illustrated in Fig. 9 at similar azimuth orientations to Fig. 7. Note that the intensity scale has been changed with respect to Fig. 7. Modeled images were found overall to have a somewhat lower return level that the measurements, so a wider dynamic range is required to obtain the full tree image. Again, lower backscatter returns from the model are expected due to the neglect of many small scale features of the tree as well as other scattering effects. The qualitative similarity between images in Figs. 7 and 9 shows that single scattering models can reproduce many features of Ka-band foliage images. This is emphasized in plot (b)

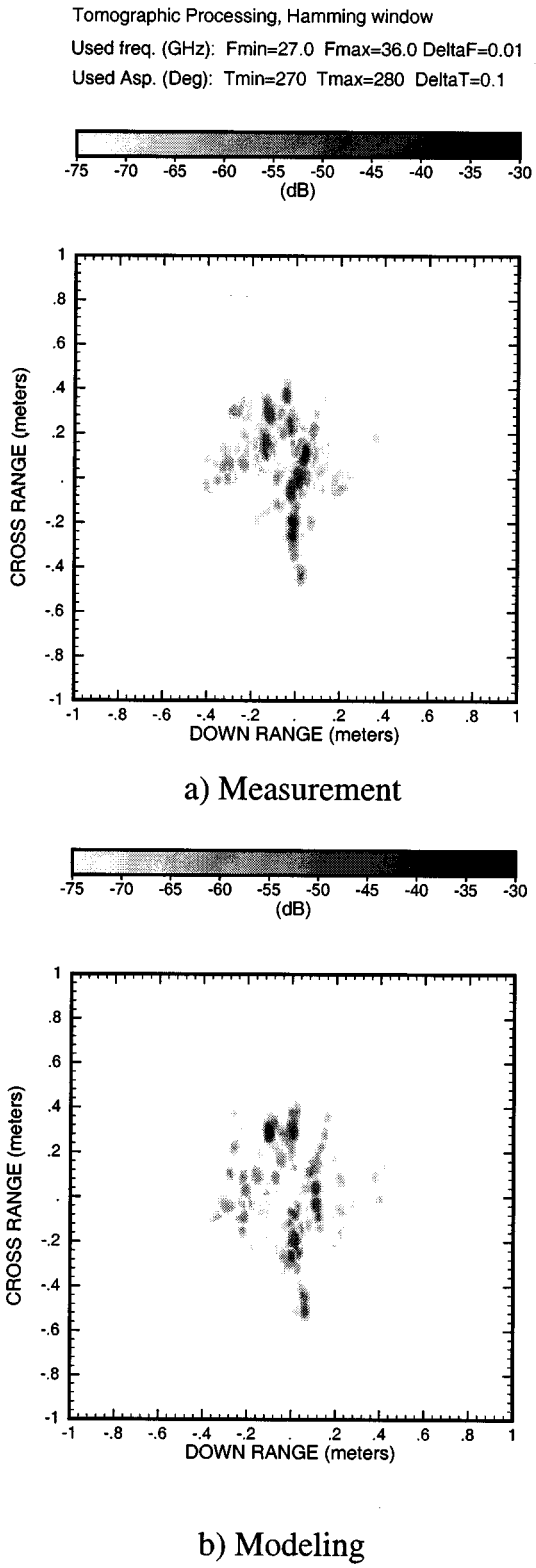


Fig. 10. Two-dimensional HV ISAR images of a bare maple tree at 270 look angle, BW = 9 GHz, $\delta f = 10$ MHz, $\Delta\theta = 10^{\circ}$, and $\delta\theta = 0.1^{\circ}$. (a) Measurement and (b) modeled.

of Fig. 8, where the tree top view and modeled image are overlaid. Again, this relatively simple model captures many of the broadside structure and branch junction returns observed in the measured image.

### *C. Bare Maple Tree: Cross-Polarized ISAR Images*

Measured and modeled cross-polarized ISAR images at a single azimuth angle are plotted in Fig. 10. Measured and modeled images have identical intensity scales in these figures, with maximum levels reduced 10 dB below the co-polarized images. Note in the measured image that the strong central trunk return observed in VV is not observed in HV, as expected for a vertically oriented cylindrical structure. Single scattered cross-polarized returns should be expected for tilted cylindrical structures and are observed to some extent in the modeled image. As discussed previously, branches in a tilted broadside orientation produce strong cross-pol backscatter returns in the model resulting in overestimation of measured results. Two such branch structures are clearly visible in the modeled image, and an examination of the tree geometry confirmed the broadside orientation of these structures. Modeled returns in other image regions are significantly smaller than the measured data, as expected, since multiple scattered returns can contribute to cross-polarized images and are not captured by the model. The reduced qualitative agreement between model and measurement in cross-polarized results should therefore be expected for a single scattering model. The relatively large level of cross-polarized backscatter obtained (only 10 dB down for some structures) illustrates that cross-polarized returns can be significant for foliage structures at Ka-band.

### *D. Leafy Maple Tree: Co-Polarized ISAR Images*

Fig. 11 plots VV ISAR images obtained for the leafy tree at four azimuth angles. The leafy tree image in Fig. 11 clearly shows a larger, more complex structure than the bare tree image in Fig. 7, since leaf scattering is an important feature at Ka-band. Some of the down range structures visible in Fig. 7 are no longer visible in Fig. 11, due to increased scattering and attenuation through the leafy canopy. To better understand attenuation effects, the 6 in diameter metallic sphere calibration target was included in the measurement, located approximately 1.2 m behind the tree center. The location of the sphere was such that it was obscured behind the tree at some azimuth angles, but not at others, as is clear from observing the sphere return as a function of azimuth in Fig. 11. It is interesting to observe in the lower left plot (centered at 305° azimuth angle) that the sphere return is relatively unattenuated even though it is located behind the tree canopy. Visual observation at this angle confirmed that the tree canopy was sparse, so that the sphere could be viewed through the tree with little obstruction. The strong radar returns obtained confirm that inhomogeneities in foliage structure can result in varying degrees of target obscuration behind a foliated object. A worst case rate of attenuation was estimated for the foliated canopy from the upper right plot, where the sphere appears almost completely obscured. It was found that approximately 17 dB of attenuation was obtained for this case.

Fig. 12(a) illustrates the model image at a single azimuth angle including the effect of the statistically described leaves discussed previously, plotted on an identical intensity scale with the measurement. Inclusion of the leaf model, even with an incomplete geometrical description, is shown to produce a striking qualitative agreement with the measured image. The more complex structure of the leafy tree compared to the bare tree is

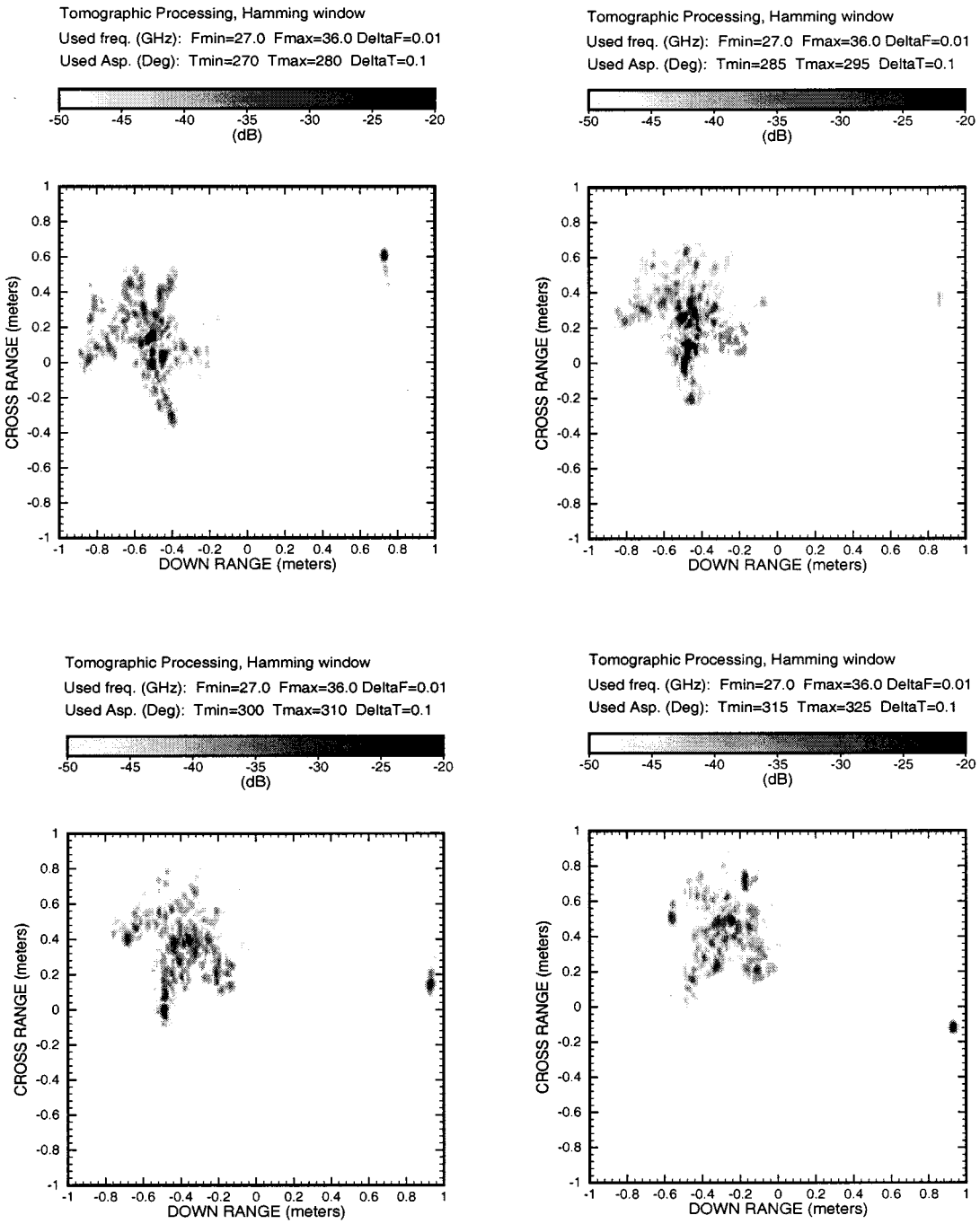


Fig. 11. Measured 2-D VV ISAR images of a leafy maple tree and a 6″ PEC sphere at various look angles: $\mathrm{BW} = 9$ GHz, $\delta f = 10$ MHz, $\Delta\theta = 10^{\circ}$, and $\delta\theta = 0.1^{\circ}$.

reproduced. However, since attenuation is not included in the single scattering model, down-range features remain strong in the modeled image compared to the measurements. A simple procedure was used to introduce attenuation effects into the model by defining an attenuation factor which depended on down range path length to each foliage object. The worst case attenuation per unit length obtained from the obscured sphere measurements was defined as $\alpha$, giving the path dependent loss as

$$L(\text{loss}) = \exp(-\alpha l) \tag{1}$$

where $l$ is the total range path length to a given scatterer. The resulting attenuation factor had a maximum of $-16.5$ dB and was applied in the model by multiplying the backscattering coefficients with this factor. Fig. 12(b) illustrates the modeled leafy tree ISAR image after applying the attenuation factor and clearly reduces down range image returns compared to the unattenuated image in plot (a). However, use of the worst case attenuation factor shows the image to be excessively attenuated compared to the measurement. A more complex model which considers the amount of foliage matter along the down range path to each scatterer could address these issues,

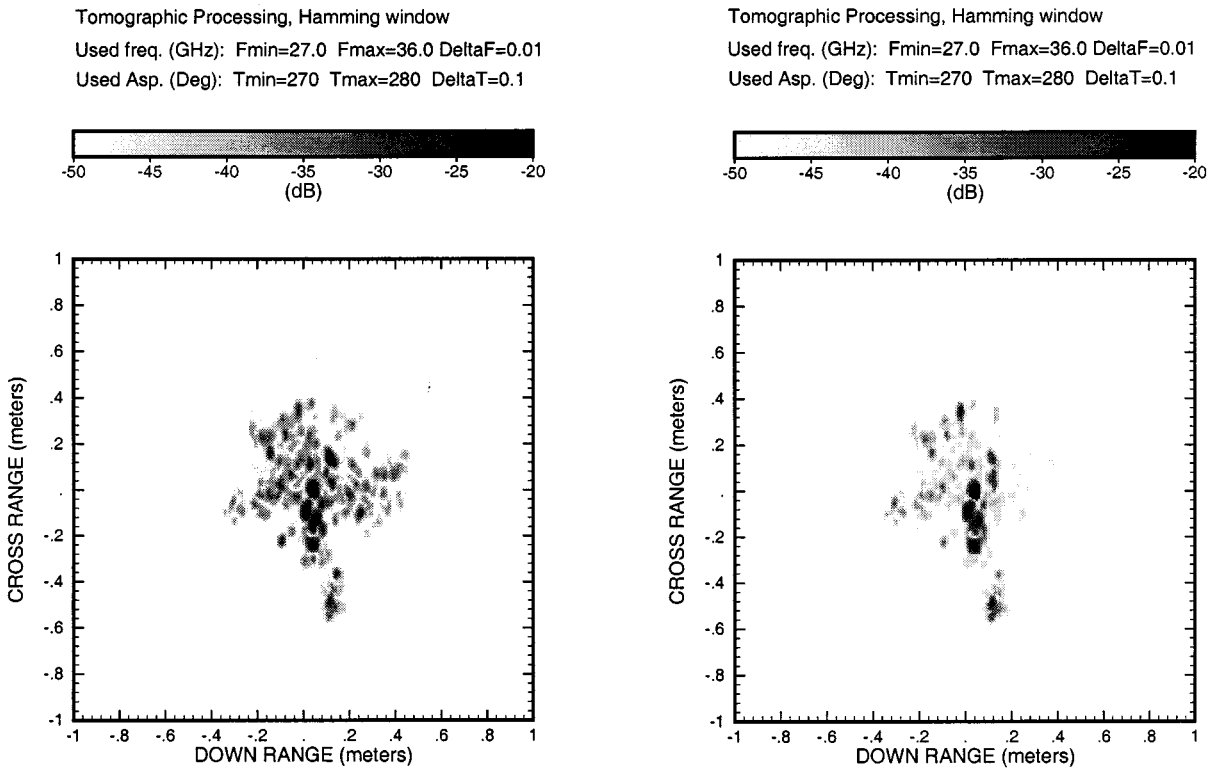


Fig. 12. Modeled 2-D copol VV ISAR image of a leafy maple tree at 270° look angle (a) without attenuation and (b) with attenuation.

but the complexity was beyond the scope of this investigation. Overall, however, the simple single scattering model again is shown to qualitatively reproduce many of the features of the measured tree image.

## V. Summary and Conclusion

High resolution Ka-band backscatter measurements for a small tree have illustrated many of the important features of foliage scattering in this frequency range. Co-polarized and cross-polarized ISAR images illustrate the influence of broadside oriented vegetation features for copol returns, and tilted cylindrical structures for cross-polarized returns. Branch junction effects are also found to be observable in measured data. Scattering from and attenuation through leaves was also observed in the ISAR images, and foliage inhomogeneities were shown to strongly influence the extent to which a target was obscured. These results confirm the importance of small scale features in Ka-band scattering from vegetation and demonstrate that the particular geometry of such features must be considered if realistic high resolution foliage images are to be simulated.

A relatively simple single scattering model was proposed and combined with detailed geometrical measurement of tree properties to produce simulated images that reproduced many of the measured image features. Limitations in geometrical knowledge of the tree structure limited a quantitative comparison, but overall results show that single scattering models can provide insight into radar images of foliage targets. The neglect of electromagnetic diffraction and multiple scattering effects was not observed to cause significant error in co-polarized image structure, and cross-polarized images also captured measured features to a lesser degree. These results motivate further Monte Carlo studies of foliage images using foliage simulation tools [18], [19] to obtain a more detailed knowledge of image statistical properties for clutter reduction and scene simulation applications.

## Acknowledgment

The authors acknowledge the assistance of Mr. T. Barnum in performing the measurements and Dr. I. J. Gupta in the use of the RIDE image processing code.

## References

[1] N. C. Currie and C. E. Brown, *Principles and Applications of Millimeter-Wave Radar*. Norwood, MA: Artech House, 1987.

[2] F. K. Shwering, E. J. Violette, and R. H. Espeland, "Millimeter-wave propagation in vegetation: Experiments and theory," *IEEE Trans. Geosci. Remote Sensing*, pp. 355–367, May 1988.

[3] M. W. Whitt and F. T. Ulaby, "Millimeter wave polarimetric measurements of artificial and natural targets," *IEEE Trans. Geosci. Remote Sensing*, pp. 562–573, Sept. 1988.

[4] F. T. Ulaby, T. Van Deventer, J. R. East, T. F. Haddock, and M. E. Coluzzi, "Millimeter wave bistatic scattering from ground and vegetation targets," *IEEE Trans. Geosci. Remote Sensing*, pp. 229–243, May 1988.

[5] S. Brown and J. C. Bennett, "High-resolution microwave polarimetric imaging of small trees," *IEEE Trans. Geosci. Remote Sensing*, vol. 37, pp. 48–53, Jan. 1999.

[6] J. Fortuny and A. J. Sieber, "Three-dimensional synthetic aperture radar imaging of a fir tree: First results," *IEEE Trans. Geosci. Remote Sensing*, vol. 37, pp. 1006–1014, Mar. 1999.

[7] M. A. Karam and A. K. Fung, "Scattering from randomly oriented circular disks with application to vegetation," *Radio Sci.*, vol. 18, pp. 557–565, July-Aug. 1983.
[8] R. K. Lang and H. A. Saleh, "Microwave inversion of leaf area and inclination angle distributions from backscattered data," *IEEE Trans. Geosci. Remote Sensing*, vol. 23, pp. 685–693, Sept. 1985.
[9] M. A. Karam and A. K. Fung, "Electromagnetic scattering from a layer of finite length, randomly oriented, dielectric, circular cylinders over a rough interface with application to vegetation," *Int. J. Remote Sensing*, vol. 9, pp. 1109–1134, 1988.
[10] K. C. McDonald, M. C. Dobson, and F. T. Ulaby, "Modeling multi-frequency diurnal backscatter from a walnut orchard," *IEEE Trans. Geosci. Remote Sensing*, vol. 29, pp. 852–863, Nov. 1991.
[11] E. Mougin, A. Lopes, M. A. Karam, and A. K. Fung, "Effect of tree structure on X-Band microwave signature of conifers," *IEEE Trans. Geosci. Remote Sensing*, vol. 31, pp. 655–666, May 1993.
[12] J. G. Fleischman, S. Ayasli, E. M. Adams, and D. R. Gosselin, "Part I: Foliage attenuation and backscatter analysis of SAR imagery," *IEEE Trans. Aerosp. Electron. Syst.*, vol. 32, pp. 135–144, Jan. 1996.
[13] T. B. A. Senior, K. Sarabandi, and F. T. Ulaby, "Measuring and modeling the backscattering cross section of a leaf," *Radio Sci.*, vol. 22, pp. 1109–1116, Nov. 1987.
[14] K. Sarabandi, T. B. A. Senior, and F. T. Ulaby, "Effect of curvature on the backscattering from a leaf," *J. Electromagn. Waves Applicat.*, vol. 2, pp. 653–670, 1988.
[15] F. T. Ulaby, R. K. Moore, and A. K. Fung, *Microwave Remote Sensing: Active and Passive*. Norwood, MA: Artech House, 1981.
[16] L. Tsang, J. A. Kong, and R. T. Shin, *Theory of Microwave Remote Sensing*. Norwood, MA: Artech House, 1985.
[17] R. H. Lang and R. Landry, "Forest backscatter modeling: Simulation versus discrete random media approach," in *Proc. Int. Geoscience and Remote Sensing Symp.*, Lincoln, NE, 1996, pp. 726–727.
[18] J. Weber and J. Penn, "Creation and rendering of realistic trees," in *ACM SIGGRAPH Conf. Proc.*, 1995, pp. 119–128.
[19] P. Prusinkiewicz and A. Lindemayer, *The Algorithmic Beauty of Plants*. New York: Springer-Verlag, 1990.
[20] G. Zhang and L. Tsang, "Wave scattering and scene image of trees generated by Lindenmayer systems," in *Proc. Int. Geoscience and Remote Sensing Symp.*, Lincoln, Nebraska, 1996, pp. 728–729.
[21] Z. Chen, L. Tsang, and G. Zhang, "Scattering of electromagnetic wave by vegetation based on the wave approach and the stochastic Lindenmayer system," *Microw. Opt. Tech. Lett.*, pp. 30–33, Jan. 1995.
[22] S. H. Yueh, "Electromagnetic and Statistical Models for Polarimetric Remote Sensing of Vegetation," Ph.D. Dissertation, Dept. EECS, Mass. Inst. Technol., Cambridge, MA, Feb. 1991.
[23] E. K. Walton and J. D. Young, "The Ohio State University compact radar cross-section measurement range," *IEEE Trans. Antennas Propagat.*, vol. AP-32, pp. 1218–1223, Nov. 1984.
[24] I. J. Gupta and A. Gandhe, "Radar Image Editing and Data Extrapolation," The Ohio State Univ. ElectroScience Lab., Columbus, Tech. Rep. 727 723-9, Apr. 1996.
[25] Y. C. Lin and K. Sarabandi, "Electromagnetic scattering model for a tree trunk above a tilted ground plane," *IEEE Trans. Geosci. Remote Sensing*, vol. 33, pp. 1063–1070, July 1995.
[26] H. Kim, J. T. Johnson, and B. Baertlein, "Backscattering from foliage at 35 GHz: Measurements and models," in *Proc. Progress in Electromagnetics Research Symp.*, Cambridge, MA, 1997, p. 772.
[27] H. Kim, J. T. Johnson, and B. Baertlein, "Ka-band backscatter measurements and modeling of tree foliage," in *Proc. Int.. Geoscience and Remote Sensing Symp.*, Seattle, WA, 1998, pp. 2086–2088.
[28] H. Kim, "Ka-Band Backscattering Measurements and Modeling of Tree Foliage," M.S. Thesis, Dept. Elect. Eng., The Ohio State Univ., Columbus, 1998.
[29] C. Matzler, "Microwave (1–100 GHz) dielectric model of leaves," *IEEE Trans. Geosci. Remote Sensing*, vol. 32, pp. 947–949, Sept. 1994.

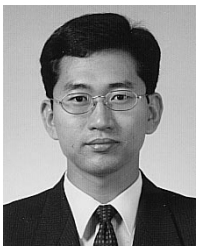

**Hyunjun Kim** was born in Seoul, Korea, in 1967. He received the B.E. and M.E. degrees in electronics engineering from Chung-Ang University, Seoul, in 1991, and 1993, respectively, and the M.S. degree in electrical engineering from The Ohio State University (OSU), Columbus, in 1998. Since 1996, he has been a Graduate Research Associate with the ElectroScience Laboratory, OSU. He is currently working toward the Ph.D. degree.

From 1995 to 1996, he was Research Staff for Korea Telecom R&D Group, Seoul, Korea, where his work involved measurement and analysis of ATM network testbed. His research interests include scattering and propagation in random media and SAR imaging of rough surface.

**Joel T. Johnson** (S'91–M'96) received the B.S.E.E. degree from the Georgia Institute of Technology, Atlanta, in 1991 and the S.M. and Ph.D. degrees from the Massachusetts Institute of Technology, Cambridge, MA, in 1993 and 1996, respectively.

He is currently an Assistant Professor, Department of Electrical Engineering and ElectroScience Laboratory, The Ohio State University, Columbus. His research interests are in the areas of microwave remote sensing, propagation, and electromagnetic wave theory.

Dr. Johnson is an associate Member of commissions B and F of the International Union of Radio Science (URSI) and a Member of Tau Beta Pi, Eta Kappa Nu, and Phi Kappa Phi. He received the 1993 best paper award from the IEEE Geoscience and Remote Sensing Society and was named an Office of Naval Research Young Investigator, National Science Foundation Career awardee, and PECASE award recipient in 1997.

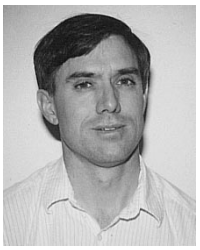

**Brian A. Baertlein** received the Ph.D. in electrical engineering from the University of Arizona, Tucson, in 1988.

His professional career includes 20 years experience in electrical engineering and applied physics comprising analyses of scattering and propagation phenomena, antenna design, electromagnetic compatibility, sensor systems of various types, sensor fusion, and signal processing. He is currently a Research Scientist with the ElectroScience Laboratory (ESL), The Ohio State University (OSU), Columbus. Before joining OSU, he was a Senior Scientist with several small businesses doing work for the U.S. DoD and DoE.